JOURNAL OF GEOPHYSICAL RESEARCH, VOL. 112, A01101, doi:10.1029/2006JA011751, 2007

Evidence for a high-energy tail associated with foreshock field-aligned beams

K. Meziane,[1] M. Wilber,[2] A. M. Hamza,[1] C. Mazelle,[3] G. K. Parks,[2] H. Rème,[3] and E. A. Lucek[4]

Received 28 March 2006; revised 15 July 2006; accepted 27 October 2006; published 6 January 2007.

[1] The reduced particle distributions of field-aligned beams observed upstream of the bow shock are examined in detail using Cluster spacecraft. We find that the reduced parallel and perpendicular distribution forms can be strongly geometry-dependent. Above a certain critical value of the angle between the local shock normal and the direction of the magnetic field, θ_{Bn}, the reduced distributions are remarkably well fit by Maxwellians. We have not found any significant changes to the spread in energies for beams at higher values of θ_{Bn}. When the angle θ_{Bn} decreases, leading to smaller beam velocities, a high-energy tail in the distribution appears. When the tail is present, the bulk of the distribution remains Maxwellian. The development of the high-energy tail is well correlated with decreases in the beam speed (or equivalently θ_{Bn}). Moreover, detailed examination of the angular distributions indicates that particles in the tails of the distributions propagate at significant pitch angles with respect to the magnetic field (are not field-aligned, as are those within the bulk of the distribution) and that these pitch angles are energy-dependent. These new observations do not fit any production mechanism expected at the shock or result from known wave-particle interactions upstream of or within the shock layer.

Citation: Meziane, K., M. Wilber, A. M. Hamza, C. Mazelle, G. K. Parks, H. Rème, and E. A. Lucek (2007), Evidence for a high-energy tail associated with foreshock field-aligned beams, *J. Geophys. Res.*, *112*, A01101, doi:10.1029/2006JA011751.

1. Introduction

[2] It is now well known that broad classes of sunward propagating ion distributions are commonly observed upstream of Earth's bow shock. Observations describing their fundamental properties have been extensively reviewed [e.g., *Thomsen et al.*, 1985]. Simulations and theoretical investigations were carried out in order to explain their production mechanisms at the shock as well as their evolution upstream [*Terasawa*, 1979; *Paschmann et al.*, 1980; *Schwartz et al.*, 1983; *Thomsen et al.*, 1983; *Burgess and Schwartz*, 1984]. The basic observational properties were first reported by *Bonifazi and Moreno* [1981a], who used data from the ISEE 2 Solar Wind Experiment, and by *Paschmann et al.* [1981], who used the ISEE 2 Fast Plasma Experiment. In particular, field-aligned ion beams (FABs) are collimated along the interplanetary magnetic field (IMF) and are observed upstream of quasi-perpendicular shocks. For these, $40° \lesssim \theta_{Bn} \lesssim 70°$, where θ_{Bn} is the angle between the IMF direction and the local bow shock normal. Their bulk energy is typically a few keV and the energy spectrum rarely extends beyond $\sim$15 keV. Their bulk speeds, ranging between 1 and several times the solar wind speed, are well correlated with θ_{Bn} [*Paschmann et al.*, 1980; *Bonifazi and Moreno*, 1981b; *Tanaka et al.*, 1983]. Downstream of the foreshock region containing FABs, intermediate and gyrating ion distributions are observed in association with large-amplitude ($\Delta B/B \sim 1$), weakly compressive ULF ($\omega/\Omega_i \ll 1$) waves [*Fuselier et al.*, 1986]. These waves propagate nearly along the ambient magnetic field direction [*Hoppe et al.*, 1981; *Meziane et al.*, 2001; *Mazelle et al.*, 2003]. The ULF waves are always absent when FABs are observed. However, whistler-like waves, commonly called foreshock 1-Hz waves, having small amplitudes ($\Delta B/B \sim 0.1$) are occasionally observed in association with FABs [*Hoppe et al.*, 1981, 1982]. These whistler wave trains have plasma rest frame frequencies of 20–100 times the proton gyrofrequency (0.5–4 Hz in the spacecraft frame of reference) and wavelengths $\sim$100 km s^{-1}. Moreover, these waves have oblique propagation directions ranging from 5° to 60° with a typical value of 45° [*Hoppe et al.*, 1982]. Careful examination of ion energy spectrograms showed that the foreshock 1-Hz waves are more often observed with FABs having a broad spread in energy, rather than with those having narrow energy ranges [*Hoppe et al.*, 1982]. From case examples, it seems that the spreading results from an extension of the energy range downward. We note that from particle observations alone the distinction between intermediate ion distributions and FABs is quite arbitrary. In practice, the simultaneous presence or lack of ULF waves is consistently used to discriminate between the two populations. In some

[1]Department of Physics, University of New Brunswick, Fredericton, New Brunswick, Canada.
[2]Space Sciences Laboratory, University of California, Berkeley, California, USA.
[3]Centre d'Etude Spatiale des Rayonnements, Toulouse, France.
[4]The Blackett Laboratory, Imperial College London, London, U.K.

0148-0227/07/2006JA011751$09.00

cases the gyrating ion distributions are observed immediately downstream of FABs, with the transition occurring within a gyroradius [*Meziane et al.*, 2004].

[3] Early FAB temperature determinations obtained an average of 345 km s^{-1}, with values extending up to $\sim$800 km s^{-1} [*Bonifazi and Moreno*, 1981a], and a temperature anisotropy $T_\perp/T_\parallel$ in the range 4–9 [*Paschmann et al.*, 1981]. The FABs are considered as the most important source of free energy in the foreshock region. The resulting ion distribution (FAB + solar wind) is unstable to numerous instabilities. The electromagnetic ion-ion cyclotron instability, discussed in detail by *Gary et al.* [1981], has the highest linear growth rate. Both the parallel and the oblique modes are unstable for a large range of FAB speeds and are in cyclotron resonance with the FABs. The parallel case has the maximum growth rate. *Gary et al.* [1981] showed that in the high-frequency range 1-Hz whistler mode waves are unstable only under specific conditions where a strong electron heat flux is present, which is typically not observed. In another theoretical study, *Wong and Goldstein* [1987] determined that FABs with a temperature anisotropy >10 should be capable of generating parallel propagating whistler waves. The observed anisotropy range of 4–9 seems to preclude this or alternatively may indicate that this instability rapidly reduces the anisotropy if initially present.

[4] Despite years of study, questions about FABs remain. Not all aspects of FAB production are understood, and the causes of the sharp spatial transition [*Meziane et al.*, 2004] between these populations and gyrating ion distributions seen in oblique geometries has not been fully examined. While the colocated ULF wave boundary indicates a clear association with the gyrating distributions, it remains unclear to what extent the shock geometry has a role in their formation. In addition, preliminary studies indicate that FABs propagating along this boundary have speeds that do not fit any known production mechanism. Careful study of the properties of the upstream populations near this transition are therefore clearly warranted, and here we begin with a detailed examination of the adjacent FABs.

[5] In the present work we examine in detail field-aligned beam distributions obtained by state-of-the-art CIS ion instruments on board Cluster and report new features not previously described. As the local shock geometry varies from quasi-perpendicular to oblique values of θ_{Bn}, a point is reached where FAB distributions show a rapid broadening of energy, and this suggests an important transition. We briefly describe the Cluster/CIS experiment in section 2 and present the observations in section 3. A discussion of the observations and a conclusion are presented in sections 4 and 5, respectively.

2. Experiment

[6] The particle data used in this study are from the Cluster Ion Spectrometer experiment, which includes (1) a Hot Ion Analyser (HIA) that measures particles in the energy range 0.005–32 $keVq^{-1}$; (2) a mass spectrometer (CODIF), which combines a top-hat electrostatic analyzer with a time-of-flight section to measure the major species H^+, He^+, He^{++} and O^+ over the energy range 0.02–38 $keVq^{-1}$. Both instruments measure full three-dimensional (3-D) distributions within one satellite spin period (4 s) with an angular resolution of 22.5° × 22.5°. In normal telemetry mode, one distribution is transmitted every 2 or 3 spins, while in burst mode a distribution is provided once every spin. Both analyzers have high and low geometry factor sections. The low geometry factor all-ion analyzer (HIA-g) records solar wind beam and magnetosheath fluxes without saturation, while the high geometry factor analyzer (HIA-G) is well-suited for measuring the orders of magnitude lower fluxes of upstream ions. Extensive descriptions of this instrument are provided in the work of *Rème et al.* [2001]. Our study also uses magnetic field data provided by the onboard fluxgate magnetometer (FGM) [*Balogh et al.*, 2001]. We have used 4 s-averaged field components to investigate the association of low-frequency waves with the backstreaming ions. The Cluster polar orbits have apogees within several R_E of the average shock location, and as a result multiple crossings are common, with most observations of upstream particles occurring in proximity to this boundary.

3. Data Selection and Observations

[7] Below we present observations obtained during three crossings of the quasi-perpendicular foreshock. In order to minimize the effect of parameters other than θ_{Bn}, each selected interval occurred during a moderately rapid, monotonic change in the IMF direction, when the upstream plasma and field conditions were otherwise steady. With the spacecraft near the shock, moderate changes in θ_{Bn} resulted in modest changes in the position on the shock where it was threaded by the spacecraft magnetic field line, and thus the angle between the solar wind direction and the shock normal, θ_{Vn}, also varied only slightly. In this way, each interval provides a good measure of the changes in upstream FABs as a function of θ_{Bn} only.

3.1. Interval 23 April 2001, 0600–0730 UT

[8] Figure 1 shows observations from 23 April 2001 between 0600 and 0730 UT, while Cluster SC 1 was at (+9.8, −15, −3.0) R_E (GSE). Figure 1a shows the proton energy spectrogram measured by CODIF at 12 s resolution. The CIS instruments were in a solar wind mode, which truncated the energy sweep for sunward look directions before reaching down to solar wind energies. Consequently, the spectra shown correspond almost exclusively to backstreaming ions. Figures 1b–1d show onboard plasma densities, velocity components, and temperatures from HIA's low geometry factor side at 4-s resolution. Finally, Figure 1e displays spin resolution GSE-components and the magnitude of the IMF measured by FGM. Figure 1 reveals a clear correlation between large-amplitude oscillations in the IMF components and the width of the proton spectra. When large-amplitude, nearly monochromatic waves are seen, the particle spectrum is wider as seen, e.g., during the 0608–0613 UT, 0619–0625 UT, and 0652–0658 UT time intervals. Detailed examination of the distributions (not shown) reveals these to be gyrating, with phase space densities (PSDs) peaked at nonzero pitch angles. In contrast, no such waves are seen when the energy spectrograms appear narrow, such as during 0615–0619 UT and 0645–0651 UT; in these cases field-aligned beams are observed. This association between low-frequency waves and backstream-

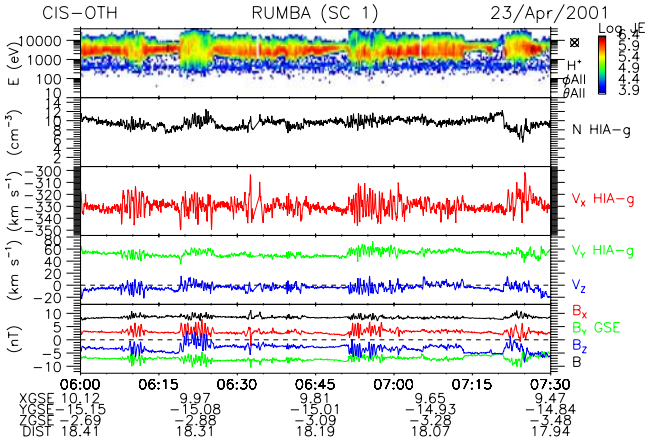

Figure 1. (a) Cluster 1 Codif spectrogram, (b–d) solar wind density and solar wind velocity, and (e) the three IMF GSE components.

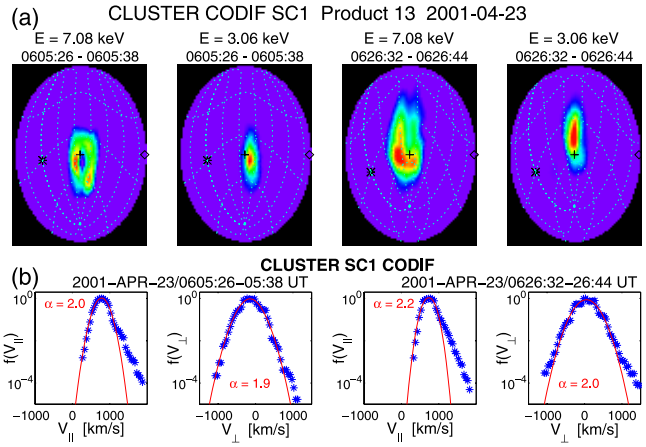

Figure 3. Same as Figure 2 for two other snapshots taken where the energy spectrogram appears wider.

ing particles is well established, and we will not discuss it further. Interestingly, Figure 1 reveals another feature, in which the proton spectra appear narrower than those observed in association with gyrating distributions but wider than those seen for field-aligned beams. For example, semibroad spectra are seen during 0601–0609 UT and 0626–0628 UT. Apparently, no large-amplitude ULF waves are observed in association with such protons. We now examine in detail the particle distributions obtained during these time intervals.

3.2. Maxwellian Field-Aligned Beams (MFABs)

[9] We begin by presenting in Figure 2 distribution functions associated with the narrow FAB spectra. Figure 2a shows the angular distributions for two snapshots taken at 0714:38–1450 UT and 0647:22–4734 UT. The Hammer-Aitoff projection [*Mailing*, 1992; *Meziane et al.*, 2001] is used to display 4π sr distributions for the individual energy channels E = 4.6 and 3.1 keV, which span the peak of the spectrum. The distributions have been rotated so that

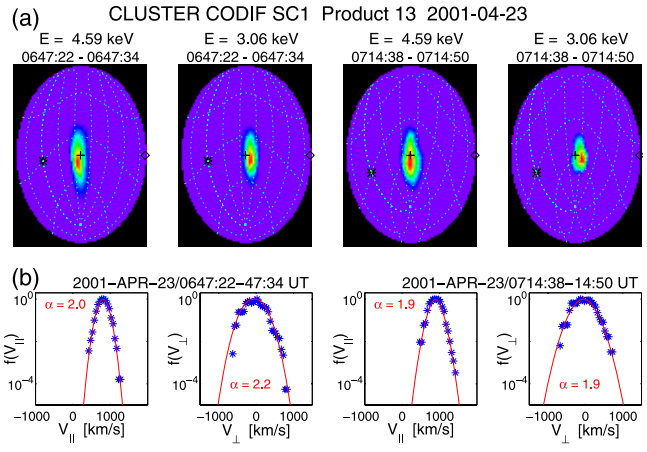

Figure 2. (a) Angular distributions plots for 3.1 keV and 4.6 keV energy channel for two distinct snapshots. (b) Corresponding reduced parallel and perpendicular distribution.

the magnetic field direction points into the page and is marked with pluses. The upstream particles shown are seen to be streaming primarily along the magnetic field direction. Each frame is effectively a projection in gyrophase (polar angle) and pitch angle (radial extent) for a single energy in the solar wind frame of reference. The antifield aligned directions are singular in these projections, located simultaneously on both the leftmost and rightmost edges. The solar wind directions are indicated by asterisks. Field-aligned propagation appears for energies near the peak of the distribution. In Figure 2b we present reduced distributions corresponding to the intervals shown in Figure 2a. The $f(V_{\|})$ plots have been obtained by integrating over perpendicular velocity space. The $f(\mathbf{v}_{\perp})$ plots have been obtained by integrating over $V_{\|}$ and the perpendicular velocity direction normal the the plane containing V_{sw} and **B**. This results in a function of the (coplanar) perpendicular velocity $\mathbf{v}_{\perp} = \mathbf{B} \times (\boldsymbol{V}_{\mathbf{sw}} \times \mathbf{B})/B^2$. Reduced distributions along the other orthogonal perpendicular axis (not shown) appear similar. The red continuous curves in Figure 2b were obtained by fitting the reduced distribution functions to a functional form $f(V) \sim \exp(-\beta V^{\alpha})$. The values obtained for the index α, indicated in each panel, are very close to 2, indicating a nearly Maxwellian fit for both $f(V_{\|})$ and $f(\mathbf{v}_{\perp})$.

[10] Figure 3 presents in the same format ion distributions during two integrations, 0605:26–0538 UT and 0626:32–2644 UT, when the energy spectrogram exhibited broader beams and no ULF waves were present. In this case the 3.1 keV protons propagate nearly along the ambient IMF direction, whereas the ~7 keV distributions show protons at nonzero pitch angles. These gyrating distributions also appear to be nongyrotropic, since the phase space densities are distributed nonuniformly among the constant pitch angle detector bins. (Time aliasing within these 3-spin integrations makes a more refined description difficult, although the discrete spots seen suggest that these are coherent gyrating distributions). It is notable that the high-energy tail is associated with the gyrating particles, while the lower-energy peak of the distribution is associated with particles moving nearly along the magnetic field direction (conventional FABs).

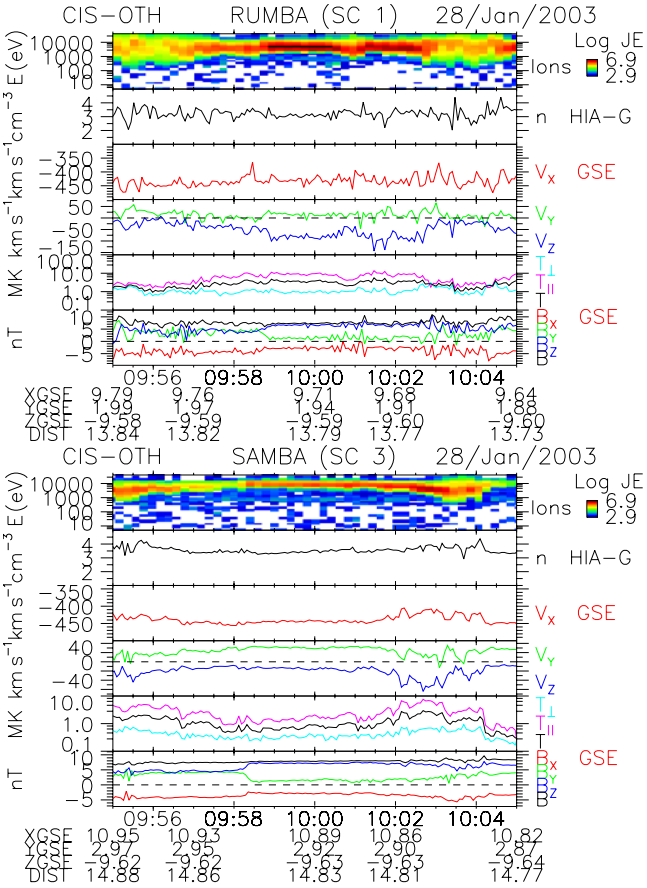

Figure 4. HIA spectrograms and IMF GSE components obtained from Cluster SC1 and SC3 for 28 January 2003.

[11] The continuous red curves in the reduced distribution functions correspond to the best fit of $f(V) \sim \exp(-\beta V^{\alpha})$. Unlike in Figure 2b, there is here a clear deviation of the curves from a quasi-Maxwellian fit for sufficiently large values of $+V_{\parallel}$ or $|\mathbf{v}_{\perp}|$. For the parallel reduced distributions we have manually assigned cutoffs at some $V_{\parallel}^{c}$ to fit only the "main beam" distributions. These $V_{\parallel}^{c}$ cutoff values depend upon the individual events and correspond to the first values where the distributions deviate from their nearly Maxwellian form. For the more symmetric perpendicular distributions, the core of the distributions could be well-modeled without similar assignment, simply by applying the fits to linear phase space densities; in this case the deviations that appear large in log plots are relatively minor. In section 3.4 we quantify the character of the energetic tails. Aside from the conspicuous high-energy tails, Figure 3b is very similar to Figure 2b. We note, however, that the two beams in this instance had speeds of 780 km s^{-1} and 734 km s^{-1}, which were slower than those for the original beams. We return to this point below when examining another time interval.

3.3. Multispacecraft Observations

[12] Figure 4 presents ion spectrograms and moments from HIA, and IMF data from FGM on SC 1 and SC 3, obtained on 28 January 2003, 0955–1005 UT. During this time, both spacecraft had nearly the same z_{GSE} coordinate (-9.62 R_E). As before, the spectrograms show upstream particles and exclude the solar wind beam. A cross section of the nominal shock taken at this value of z_{GSE}, with the projected locations of SC 1 and SC 3 onto the ecliptic plane, is shown in Figure 5. Because of a significant separation, the two spacecraft do not observe the same features. It is clear that for most of the interval the energy spectrogram corresponding to the backstreaming particles appears narrower for SC 3 than for SC 1. We want to examine the particle distributions between 0959 and 1000 UT, where no ULF waves are observed in either spacecraft. During this time interval the average IMF direction in the ecliptic plane is also indicated in Figure 5 illustrating the magnetic connection to the shock. Clearly, SC 3 is shock connected upstream of SC 1.

[13] The reduced parallel particle distribution functions of the FABs observed simultaneously by spacecraft 1 and 3 are shown in Figure 6. For clarity, the continuous curves show the best fits to Maxwellians ($\alpha = 2$). These fits seem satisfactory for the FAB observed at SC 3, whereas the FAB observed by SC 1 exhibits a high-energy tail. In agreement with the previous events, the Maxwellian distribution has a peak phase space density at a higher velocity ($V_{\parallel}^{SC3} = -1200$ km s^{-1}) than seen for the peak phase space density of the non-Maxwellian FAB ($V_{\parallel}^{SC1} = -936$ km s^{-1}). The dashed vertical line in both panels on the left indicates $V_{\parallel} = -936$ km s^{-1}, the peak value for the latter distribution.

3.4. The α Index-Beam Speed Correlation

[14] In this section we examine in detail the high-energy tail associated with the FABs. We consider a time interval during which the FABs exhibited rapid speed fluctuations. As before, a requirement for our data selection included an absence of ULF wave activity.

[15] Figure 7 shows successive reduced parallel distribution functions of FABs observed by SC 1 on 22 January

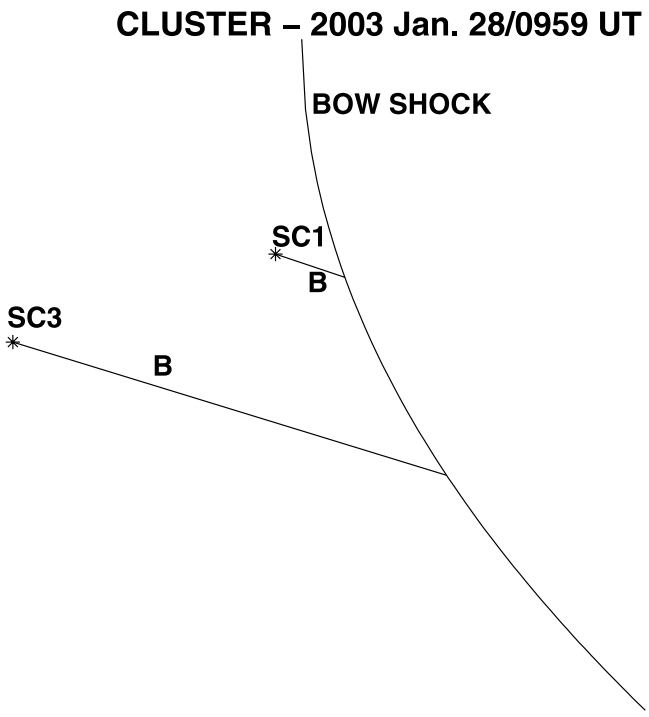

Figure 5. Cross section bow shock schematic and position of CLUSTER 1 and 3 on 28 January 2003 at 0959:20 UT.

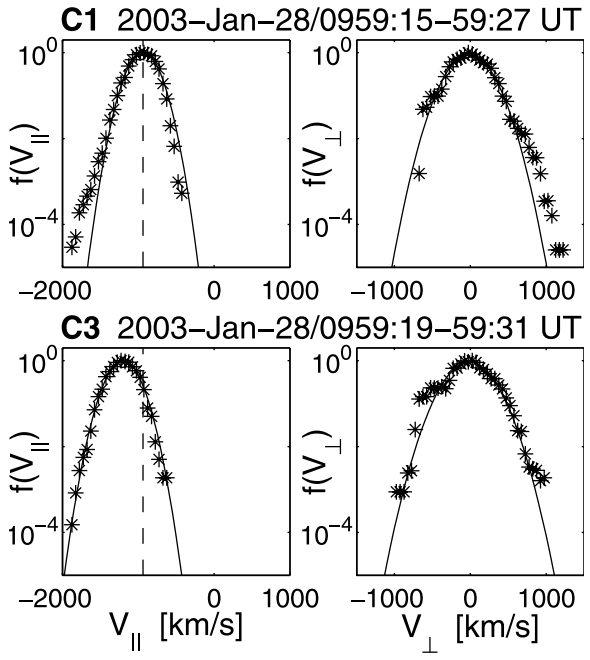

Figure 6. Reduced distributions functions obtained from (top) SC1 and (bottom) SC3 for 28 January 2003.

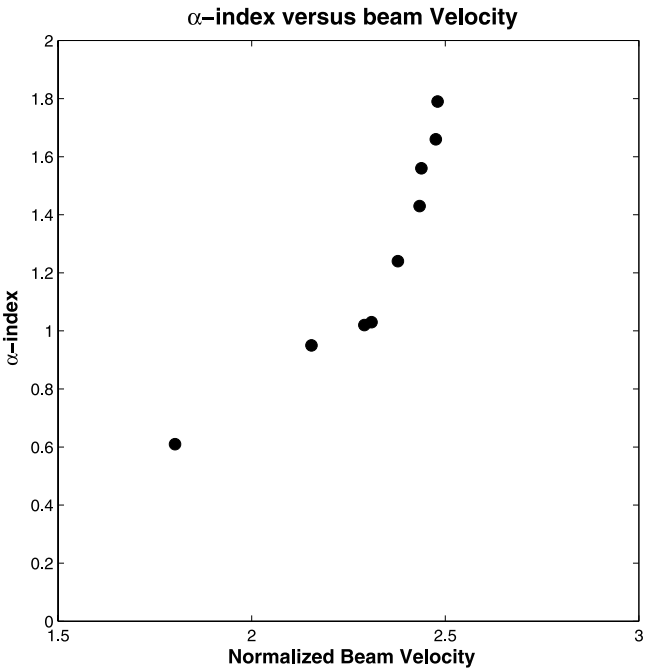

Figure 8. The stretch exponential index α versus normalized parallel beam velocity.

2004. The beam parallel speeds are particularly high. However, when normalized to the solar wind speed, which is relatively high during this event ($V_{sw} \sim 650$ km s^{-1}), the beams have typical speeds. Clearly, the distribution functions in Figure 7 present profiles with variously developed high energy tails and different beam speeds. As in Figure 3b, we fit each distribution excluding the high-energy tail (dashed curve), although in these cases α is fixed at 2. Similar to those events, when the tail is absent or weakly present, a Maxwellian function is a satisfactory fit for the distribution.

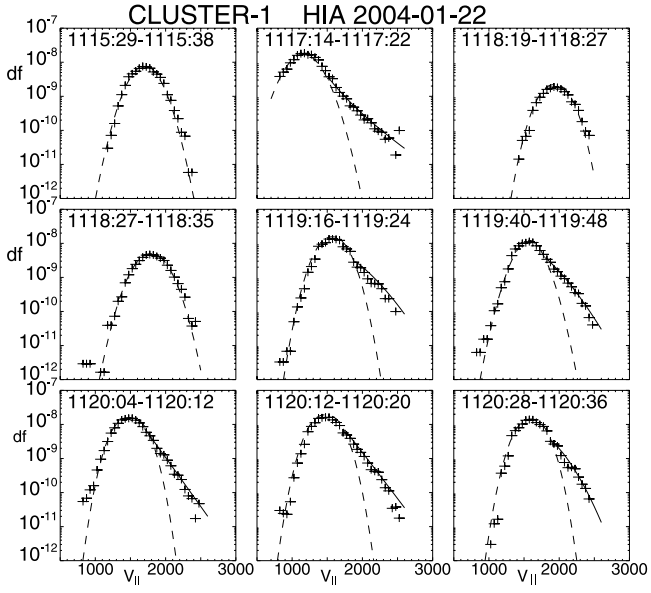

Figure 7. Successive reduced parallel distributions obtained by SC1-HIA on 22 January 2004 between 1116:26 and 1120:04 UT.

[16] In order to quantify the characteristics of the high-energy tails, we fit those points above the $V_{\|}^{c}$ cutoff used to limit the (red) Maxwellians in Figure 7 to the functional form $f(V) \sim \exp(-\beta V^{\alpha})$. When the energetic tails are present, these best-fits are plotted as continuous curves. We have found that the tail fit result is robust even when $V_{\|}^{c}$ is varied as much as 50–100 km s^{-1}. Figure 7 suggests a strong relationship between the hardness of the tail and the normalized bulk beam speed. This is demonstrated more explicitly in Figure 8, which plots the values of α obtained from the best tail fits versus the normalized beam speeds $P_{\|} = V_{b\|}/V_{sw}$, for $V_{b\|}$ the beam parallel speeds.

[17] The beam speeds vary with changes in the shock geometry, which result as the IMF rotates. It is well known that the FAB speed varies according to $P_{\|} \sim 1/\cos\theta_{Bn}$ [*Schwartz et al.*, 1983]; thus the changes in the the beam speed are a good indicator of the θ_{Bn} changes. Usually, this angle is estimated at locations away from the shock by employing semiempirical bow shock models, which have been determined using averages of observed shock crossing positions. In practice, the true positions deviate significantly from the model values, and the computed θ_{Bn} values show correspondingly large errors. Here we use $V_{b\|}$ as a proxy for θ_{Bn}. (We remind the reader here that we selected events that would minimize the variation of parameters other than θ_{Bn}.) Six of the corresponding distributions are shown in Figure 7; those not shown were obtained from adjacent intervals. Figure 8 shows a clear trend indicating that the high-energy tail is more developed ($\alpha \rightarrow \sim 0$) as the beam velocity decreases.

[18] The results presented in Figure 3a indicates that the particles composing the tail of the distribution have a significant motion perpendicular to the magnetic field

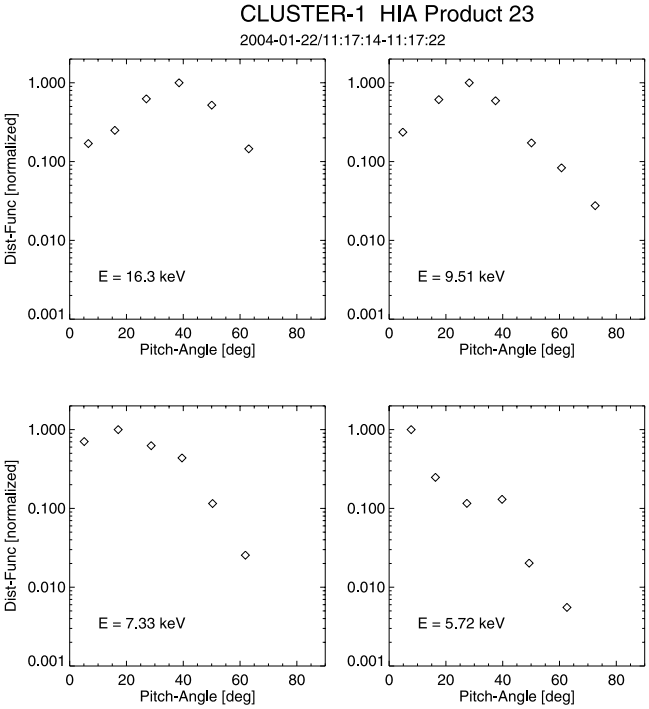

Figure 9. Pitch angle distributions for four energy channels when FAB high-energy tail is present.

direction. In order to quantify this, we plot the pitch angle distributions for different energy channels for two of the distributions presented in Figure 7 above. The pitch angle distributions in four energy channels for 1117:14–17:22 UT and 1118:27–18:35 UT are shown are shown in Figures 9 and 10, respectively. These were computed after translating the distributions into the plasma rest frame, with phase space densities averaged over 11.25° bins (corresponding roughly to the detector angular resolution). In the first snapshot, where the velocity space distribution exhibits a significant high-energy tail (α = 0.94), only the lower-energy ($E < 5.72$ keVq^{-1}) ions are field-aligned; ions with energy $E \geq 7.33$ keVq^{-1} have a significant motion perpendicular to the magnetic field, showing that the pitch angle of the PSD maximum is energy-dependent. For the second interval (Figure 10), which was seen to have no tail (α = 2.1), only the $E \geq 14.6$ keVq^{-1} channel has a noticeable perpendicular speed.

4. Discussion

[19] We have presented the first observations of foreshock ion distributions that are primarily field-aligned but which also exhibit nonthermal tails in the absence of significant ULF wave activity. When the shock geometry is quasi-perpendicular well-known field-aligned beams are seen, which have reduced distributions $f(V_{\|})$ and $f(\mathbf{v}_{\perp})$ that are Maxwellian. At some point as θ_{Bn} is decreased nonthermal tails appear, with the main distributions retaining their Maxwellian form. Further decreases in θ_{Bn} lead to a hardening of the nonthermal tails, which are not field-aligned and are nongyrotropic, with the most energetic ions having the largest pitch angles.

[20] If we consider the known mechanisms in the literature for upstream ion production there are difficulties in accounting for the nonthermal tails. A leading current idea about FAB production is that they originate in the gyrating ion distribution present in the foot of the shock, which results as a fraction of incoming solar wind ions are reflected in the shock's macroscopic fields. These particles attain their beam energies as they gyrate along the direction of the solar wind electric field following initial reflection. This model requires a yet-to-be identified pitch angle scattering mechanism, which is necessary to put specularly reflected ions into regions of velocity space directly accessible to the upstream [*Möbius et al.*, 2001; *Kucharek et al.*, 2004]. The rather vigorous scattering required to place significant particles fluxes into the velocity space escape cone apparently produces a homogeneous pitch angle distribution when FABs are seen. As a means of producing the high-energy tails shown here, it is problematic. As θ_{Bn} decreases, it is possible that the scattering at higher energies becomes less vigorous, resulting in a pitch angle gradient. This could produce a nongyrotropic energetic component, although the strong gradient required to produce a gyrating population with low fluxes along the field direction seems unlikely to produce sufficient particles within the escape cone to match the observations. Furthermore, there is no reason to expect such a scattering mechanism to produce a nonthermal tail or to turn on this capacity at some critical θ_{Bn} angle.

[21] In the shock drift acceleration model, the particles gain energy as they drift along the shock surface in the direction of the motional electric field. The energization efficiencies as well as the emergent particle pitch angle distributions are strongly θ_{Bn} dependent. The model predicts

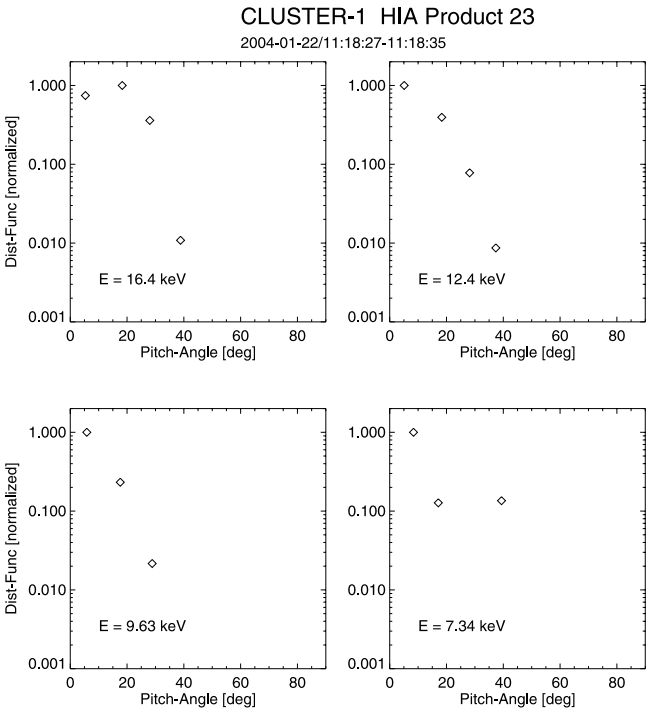

Figure 10. Pitch angle distributions for four energy channels in absence of FAB high-energy tail.

that the pitch angle for the peak of the distribution should increase with θ_{Bn} and that the distribution should harden, both of which are opposite to the observations that we present. This casts doubt on shock drift acceleration as the mechanism producing these particles.

[22] *Edmiston et al.* [1982] considered the possibility that upstream ions result from adiabatic (μ conserving) escape of particles from the thermal tail of magnetosheath distributions. They predicted significant upstream fluxes for quasi-parallel shocks but too few escaping ions to produce the FABs observed in quasi-perpendicular regions. Were the fluxes high enough to produce the nonthermal tails in oblique geometries, they would lead to field-aligned distributions with $T_{\|} > T_{\perp}$, rather than gyrating distributions. *Schwartz et al.* [1983] discussed a magnetosheath leakage idea, where $\mathbf{v} \cdot \mathbf{n}$ is conserved, rather than μ. This would produce nongyrotropic distributions upstream but has yet to be observed. There is nothing in the simple statement of this model that favors the escape of energetic particles with larger pitch angles, however. While the specular reflection picture predicts a PSD maximum at a pitch-angle equal to θ_{Bn} in the plasma frame and this will produce a pitch angle distribution that is independant upon energy.

[23] When considering the possibility of energetic magnetospheric ion leakage as a source for the nonthermal tails, it is important to note that the field lines threading the spacecraft must thread the magnetopause. For the case presented in Figure 1 this seems unlikely, given the large IMF_z component and a spacecraft location near the equatorial plane. We have examined data from the ion composition instrument (CODIF) for the above time intervals and have found no indication of magnetospheric tracer particles such as He^+ or O^+ above 5 $keVq^{-1}$. The absence of a clear He^+ signature itself is inconclusive, however, since this species is not well separated from H^+ and He^{++} at these energies.

[24] *Tanaka et al.* [1983] proposed an alternative FAB production mechanism, for which the quasi-trapped gyrating ions produced by shock reflection excite electromagnetic ion cyclotron instabilities downstream. These in turn scatter magnetosheath ions into velocity space domains accessible to the upstream. In their simulations they obtained distributions peaked at nonzero pitch angles for oblique geometries, rather than the FABs seen when θ_{Bn} is larger. Because those simulations were computed for conditions different from those observed in our case, we cannot make a direct comparison with our results. A general difficulty with the *Tanaka et al.* [1983] model, however, is that it exhibits a decrease in backstreaming fluxes as θ_{Bn} decreases, which is not observed.

[25] If the nonthermal tail ions originate from within the downstream side of the shock, we should expect them to produce field-aligned distributions in cases where they approximately conserve μ when crossing the shock. However, under the combined influence of the magnetic mirror force and the cross shock potential, these particles should emerge from the shock with smaller pitch angles, and the emergent pitch angle should be approximately energy-independent.

[26] Some care must be taken when considering the sources of the particles constituting these distributions, since velocity filtering occurs. Differing parallel speeds imply different connection times at the shock for simultaneously observed ions, and this in turn leads to longer convection times at solar wind perpendicular velocities $\mathbf{V}_{sw\perp}$ for those that are slower. The result are shock intercepts further upstream for particles with low $V_{\|}$, leading to variation in the source shock geometry. We have used three bow shock models to examine the possible effects of this differing travel time for the 23 April crossing, each producing qualitatively similar results. For the purpose of illustration, we briefly discuss the results from the model due to *Cairns et al.* [1995], which returned θ_{Bn} values that were intermediate between those from the other models [*Farris et al.*, 1991; *Slavin and Holzer*, 1981]. Because it placed Cluster at the largest shock distances this model is least likely to have underestimated the effects of shock travel time. At 0605:32 UT, when a nonthermal tail distribution was observed, the estimated shock distance was 4 R_E. The 784 km s^{-1} peak beam speed required a travel time of 33 s, while the largest measured parallel speed was 1850 km s^{-1}, requiring a substantially shorter travel time. With $\mathbf{V}_{sw\perp}$ = (−230, −75, −80) km s^{-1}, the convection difference would be of the order of an R_E.

[27] By iteratively solving for the model shock parameters and the particle connection point, taking into consideration the time required for the measured solar wind conditions to convect to the shock intercept, and for the beam to travel from there to the spacecraft, we found that the peak of the beam originated at (11.8, −10.6, −0.6) R_E with $\theta_{Bn} = 44.9°$, while for a nonthermal tail particle with $V_{\|}$ = 1100 km s^{-1} the source was located at (11.3, −12.0, −1.7) R_E with $\theta_{Bn} = 42.0°$. A sharp transition between field-aligned beams and gyrating distributions can occur at oblique geometries [*Meziane et al.*, 2004], but if this accounts for the high-$V_{\|}$ particles, we should expect to see nonthermal tails less frequently for more radial IMF orientations, when the convection distances are negligible. A preliminary look for this effect does not seem to bear out the correspondence.

[28] We note that the observations here otherwise appear inconsistent with the picture presented by *Meziane et al.* [2004], in which FABs were observed simultaneously with "remotely sensed" gyrating distributions having guiding centers located on adjacent field lines less than a gyroradius downstream. A case against remote sensing is seen in the distribution for 0605:26–0605:38 UT (Figure 3). The reduced distribution for $f(V_{\|})$ (lower left) shows a Maxwellian distribution below 1050 km s^{-1} and a nonthermal tail above this speed, with the angular distribution for 3.1 keV (second top panel) showing a field-aligned population. The simultaneously observed 7.1 keV angular distribution shows a full annulus, indicating particles of all gyrophases, and therefore arriving from all directions perpendicular to **B**, rather than from a restricted range. Another signature present in the 3 February 2001 event from Figure 1 of the earlier paper could be seen in the energy flux spectrogram. There a FAB spectrum centered on a few $keVq^{-1}$ was joined by a more energetic spectrum near 20 $keVq^{-1}$. The two spectra merged as the region populated with gyrating ions was approached, with first the larger gyroradius ions being sampled, followed by those with decreasing energy (and gyroradii). This signature is not observed in any of the nonthermal tail cases presented here.

[29] Another possibility is that the observed distributions originate as field-aligned beams, but are modified locally, or enroute from the shock to the spacecraft. The lack of significant wave power at the spacecraft seems to rule out local modification. The orientation of the ULF wave boundary predicted by *Skadron et al.* [1988] is at an angle relative to $\hat{x}_{GSE}$ larger than that for the IMF. This permits a geometry where there may be significant ULF wave activity in between the shock and the spacecraft, even when none is seen where the particles are detected. This possibility is difficult to maintain for two reasons. First, there is no record of FABs observed simultaneously with ULF waves at any distance from the shock. The existence of an inner FAB boundary reported in the recent study by *Meziane et al.* [2004] is consistent with this established result. Our examination of a limited number of foreshock crossings suggests that the nonthermal energetic tails are a feature commonly associated with foreshock FABs, rather than something specific to particular events. Second, if an ion beam encounters a region of high ULF wave activity these particles certainly will be affected, but no known mechanism predicts a systematic energization leading to the formation of a tail.

[30] Additionally, the possibility that the FAB tails result from resonant processes involving wave-particle interaction taking place within the shock layer is not a suitable explanation. At quasi-perpendicular shock geometries, FAB production is supposed to result from scattering process, leading to nearly Gaussian distribution profiles. The observed electromagnetic and electrostatic turbulence is significantly more important at oblique shocks and lower values of θ_{Bn}, leading to higher scattering than in quasi-perpendicular conditions. In diffusive processes it is not expected, according to the limit central theorem, that the distribution will change from nearly Maxwellian to a skewed shape, i.e., the resulting particle distribution should retain a broader, but still nearly Maxwellian shape. This clearly contrasts with the data presented here.

[31] Finally, it is often found in laboratory and space plasmas that the probability distribution functions (PDF) are Gaussian near their centers, but have tails that deviate significantly from this form. Early studies of wave-particle interaction, using weak turbulence theory, all suggested a broadening of the distribution function. Strong turbulence theories are perturbative theories that are limited, in most cases, by closures. In the past decade, nonperturbative techniques, borrowed from field theory and applied to fluid and plasma turbulence problems, have linked non-Gaussian features in the PDFs to intermittency and to coherent spatiotemporal structures. *Batchelor and Townsend* [1949] were probably the first to point out that the small scales of high Reynolds number turbulence are intermittent; in other words, that high-frequency or high wave number turbulent activity manifests itself in bursts separated by long relatively quiescent periods. It is now believed that the tails are the product of intermittency due to rare events of large amplitude, that they are likely to arise from bursty events or the development of nonlinear coherent structures.

[32] Intermittent physical processes at the collisionless shocks are predicted by both hybrid and full particle simulations [*Winske and Quest*, 1988; *Lembège and Savoini*, 1992]. These simulations have shown the occurrence of time variability in the shock microstructure leading to magnetic field variation on the order of 20%, on timescales on the order of the local gyroperiod. In fact, depending on the Alfvenic Mach number M_A and upstream β plasma, the magnetic field variation could be higher. Shock self-reformation occurs because of an accumulation of reflected ions in the foot of the shock and associated currents that increase the magnetic field there. A structure standing in front of the main ramp grows and ultimately replaces the original shock front, within time spans on the order of an ion gyroperiod. At the various stages of this process, the local shock strength and associated cross shock potential varies, along with the direction of the normal, changing the associated ion reflection efficiency. Consequently, a self-reforming shock follows a quasi-intermittent pattern. It is likely that this process will have significant consequences on the escaping upstream particle distribution, with the details being unresolved by the current capabilities of ion analyzers. Therefore higher time resolution ion measurements, as expected for MMS, are needed in order to allow for a straightforward test of this self-reformation picture.

[33] The nonstationarity behavior of shocks is expected to be θ_{Bn} dependent, particularly as this affects ion reflection efficiencies. For oblique shocks, the specularly reflected ion density has not always been found to be sufficient for producing shock self-reformation in simulations, suggesting stability (e.g., *Lembège and Savoini* [1992], whose $2\frac{1}{2}$-D full particle simulations, using an ion/electron mass ratio of 42, produced no self-reformation at θ_{Bn} angles below 62°). However, a recent 1-D full particle simulation of a quasi-perpendicular shock using a realistic electron to proton mass ratio indicates that shock reformation processes may still occur for oblique shocks [*Scholer and Matsukiyo*, 2005]. The occurrence of the shock reformation for these geometries results from a two-stream instability which occurs as long as the shock specularly reflects a significant fraction of incoming solar wind ions. Although shock self-reformation resulting from particle reflection is well-established in simulation studies [*Hada et al.*, 2003], observational evidence is still lacking. We believe that the new FAB features reported in the present study are worth investigating in the context of shock self-reformation.

5. Conclusions

[34] In this paper we have examined in detail the particle distributions of field-aligned beams observed upstream of the bow shock by the Cluster spacecraft. We have found that the characteristics of both parallel and perpendicular particle distribution function profiles are geometry-dependent. Above a critical θ_{Bn} value, the reduced distributions are well-fit by Maxwellians. For smaller θ_{Bn} the reduced distribution functions exhibit nonthermal high-energy tails which harden as θ_{Bn} is reduced. The angular distributions associated with the high-energy tails indicate that these components are nongyrotropic. We have found that the occurrence of such high-energy tails does not agree with any known shock-acceleration or wave-particle interaction mechanisms.

[35] The nongyrotropic character of ions in the tails of the FAB distributions shown here, in combination with the fact

that these are seen only in oblique geometries is strongly suggestive of a link between FABs and gyrating ion distributions. It is well established that gyrating ion distributions most often appear nongyrotropic also and are seen in the presence of nearly monochromatic ULF waves. They are always observed near the inner (low-θ_{Bn}) boundary of FABs [*Meziane et al.*, 2004]. It is now believed that gyrating ion distributions result from wave trapping of FAB ions. This interpretation is based upon direct comparison between theory and observation, often with an excellent match for both the Doppler shifted wave frequencies and the pitch angles for the peaks of the gyrating ion distributions [*Meziane et al.*, 2001; *Mazelle et al.*, 2003]. Not all gyrating ion distributions match the predicted pitch angles, however, and generally these populations are considerably hotter than FABs. We are currently extending the present study to examine the dependencies of pitch angles as a function of energy for gyrating ion distributions in order to determine whether there is a relationship to the high-energy tails in the FABs presented here.

[36] **Acknowledgments.** Work at UNB is supported by the Canadian Natural Science and Engineering Council. K.M is grateful to the International Space Science Institute for providing the opportunity and support to discuss problems related to the foreshock. Part of the work of K. M. has been supported funding from Observatoire Midi-Pyrénées. Work at U. C. Berkeley is supported by NASA grant NAG5-10131.

[37] Zuyin Pu thanks the reviewers for their assistance in evaluating this paper.

References

Balogh, A., et al. (2001), The cluster magnetic field investigation: Overview of in-flight performance and initial results, *Ann. Geophys.*, *19*, 1207.

Batchelor, G. K., and A. A. Townsend (1949), The nature of turbulent motion at large wave-numbers, in *Proc. R. Soc. London*, *199*, 238.

Bonifazi, C., and G. Moreno (1981a), Reflected and diffuse ions backstreaming from the Earth's bow shock: 1. Basic properties, *J. Geophys. Res.*, *86*, 4381.

Bonifazi, C., and G. Moreno (1981b), Reflected and diffuse ions backstreaming from the Earth's bow shock: 2. Origin, *J. Geophys. Res.*, *86*, 4397.

Burgess, D., and S. J. Schwartz (1984), The dynamics and upstream distributions of ions reflected at the Earth's bow shock, *J. Geophys. Res.*, *89*, 7407.

Cairns, I. H., D. H. Fairfield, R. R. Anderson, V. E. H. Carlton, K. I. Paularena, and A. J. Lazarus (1995), Unusual locations of Earth's bow shock on September 24–25, 1987: Mach number effects, *J. Geophys. Res.*, *100*, 47.

Edmiston, J. P., C. F. Kennel, and D. Eichler (1982), Escape of heated ions upstream of quasi-parallel shocks, *Geophys. Res. Lett.*, *9*, 531.

Farris, M. H., S. M. Petrinec, and C. T. Russell (1991), The thickness of the magnetosheath: Constraints on the polytropic index, *Geophys. Res. Lett.*, *18*, 1821.

Fuselier, S. A., M. F. Thomsen, J. T. Gosling, S. J. Bame, and C. T. Russell (1986), Gyrating and intermediate ion distributions upstream from the Earth's bow shock, *J. Geophys. Res.*, *91*, 91.

Gary, S. P., J. T. Gosling, and D. W. Forslund (1981), The electromagnetic ion beam instability upstream of the Earth's bow shock, *J. Geophys. Res.*, *86*, 6691.

Hada, T., M. Onishi, B. Lembège, and P. Savoini (2003), Shock front nonstationarity of supercritical perpendicular shocks, *J. Geophys. Res.*, *108*(A6), 1233, doi:10.1029/2002JA009339.

Hoppe, M. M., C. T. Russell, L. A. Frank, E. W. Eastman, and T. E. Greenstadt (1981), Upstream hydromagnetic waves and their association with backstreaming ion populations: ISEE 1 and 2 observations, *J. Geophys. Res.*, *86*, 4471.

Hoppe, M. M., C. T. Russell, T. E. Eastman, and L. A. Frank (1982), Characteristics of the ULF waves associated with upstream ion beams, *J. Geophys. Res.*, *87*, 643.

Kucharek, H., E. Möbius, E. Scholer, C. Mouikis, L. M. Kistler, T. Horbury, A. Balogh, and H. Rème (2004), On the origin of field-aligned beams at the quasi-perpendicular shock: Multispacecraft obervations by Cluster, *Ann. Geophys.*, *22*, 2301.

Lembège, P., and P. Savoini (1992), Nonstationarity of a two-dimensional quasiperpendicular supercritical collisionless shock by self-reformation, *Phys. Fluids B*, *4*, 3533.

Mailing, D. H. (1992), *Coordinate Systems and Map Projections*, 2nd ed., Elsevier, New York.

Mazelle, C., et al. (2003), Production of gyrating ions from nonlinear wave-particle interaction upstream from the Earth's bow shock: A case study from Cluster-CIS, *Planet. Space Sci.*, *51*, 785.

Meziane, K., C. Mazelle, R. P. Lin, D. LeQuéau, D. E. Larson, G. K. Parks, and R. P. Lepping (2001), Three-dimensional observations of gyrating ion distributions far upstream from the Earth's bow shock and their associated with low-frequency waves, *J. Geophys. Res.*, *106*, 5731.

Meziane, K., et al. (2004), Simultaneous observations of field-aligned beams and gyrating ions in the terrestrial foreshock, *J. Geophys. Res.*, *109*, A05107, doi:10.1029/2003JA010374.

Möbius, E., et al. (2001), Observations of the spatial and temporal structure of field-aligned beam and gyrating ring distributions at the quasi-perpendicular bow shock with Cluster CIS, *Ann. Geophys.*, *19*, 1411.

Paschmann, G., N. Sckopke, J. R. Asbridge, S. J. Bame, and J. T. Gosling (1980), Energization of solar wind ions by reflection from the Earth's bow shock, *J. Geophys. Res.*, *85*, 4689.

Paschmann, G., N. Sckopke, I. Papamastorakis, J. R. Asbridge, S. J. Bame, and J. T. Gosling (1981), Characteristics of reflected and diffuse ions upstream from the Earth's bow shock, *J. Geophys. Res.*, *86*, 4355.

Rème, H., et al. (2001), First multispacecraft ion measurements in and near the Earth's magnetosphere with identical Cluster ion spectrometry (CIS) experiment, *Ann. Geophys.*, *19*, 1303.

Scholer, M., and S. Matsukiyo (2005), On kinetic structure of quasi-pependicular collisionless shocks, in *The Physics of Collisionless Shocks, 4th Annual IGPP International Astrophysics Conference*, *AIP Conf. Proc. Ser.*, vol. 781, edited by G. Li, G. P. Zank, and C. T. Russell, pp. 22–26, Am. Inst. of Phys., Melville, N. Y.

Schwartz, S. J., M. F. Thomsen, and J. T. Gosling (1983), Ions upstream of the Earth's bow shock: A theoretical comparison of alternative source populations, *J. Geophys. Res.*, *88*, 2039.

Skadron, G., R. T. Holdaway, and M. A. Lee (1988), Formation of the wave compressional boundary in the Earth's foreshock, *J. Geophys. Res.*, *93*, 11,354.

Slavin, J. H., and R. E. Holzer (1981), Solar wind flow about terrestrial planets: 1. Modeling bow shock position and shape, *J. Geophys. Res.*, *86*, 11,401.

Tanaka, M., C. C. Goodrich, D. Winske, and K. Papadopoulos (1983), A source of the backstreaming ion beams in the foreshock region, *J. Geophys. Res.*, *88*, 3046.

Terasawa, T. (1979), Origin of 30 $\sim$ 100 kev protons observed in the upstream region of the Earth's bow shock, *Planet. Space Sci.*, *27*, 365.

Thomsen, M. F., S. J. Schwartz, and J. T. Gosling (1983), Observational evidence on the origin ions upstream of the Earth's bow shock, *J. Geophys. Res.*, *88*, 7843.

Thomsen, M. F., J. T. Gosling, S. J. Bame, and C. T. Russell (1985), Gyrating ions and large-amplitude monochromatic MHD waves upstream of the Earth's bow shock, *J. Geophys. Res.*, *90*, 267.

Winske, D., and K. B. Quest (1988), Magnetic field and density fluctuations at perpendicular supercritical collisionless, *J. Geophys. Res.*, *93*, 9681.

Wong, H. K., and M. L. Goldstein (1987), Proton beam generation of whistler waves in the Earth's bow shock, *J. Geophys. Res.*, *92*, 12,419.

A. M. Hamza and K. Meziane, Physics Department, University of New Brunswick, Fredericton, NB, E3B 5A3, Canada. (karim@unb.ca)

E. A. Lucek, Blackett Laboratory, Imperial College, London, SW7 2BW, UK.

C. Mazelle and H. Rème, Centre d'Etude Spatiale des Rayonnements, 9 Ave. du Colonel Roche, Toulouse F-31028, France.

G. K. Parks and M. Wilber, Space Sciences Laboratory, University of California, Berkeley, CA 94720, USA.